Stability Analysis of a Novel Switched Inductor Based Quadratic Boost DC-DC Converter

Divya Navamani JAYACHANDRAN, Vijayakumar KRISHNASAMY, Jegatheesan RAMIAH

Department of Electrical and Electronics Engineering, School of Electrical and Electronics Engineering, SRM University, Kancheepuram District, 603 203 Kattankulathur, India

divyateddy1@gmail.com, kvijay_srm@rediffmail.com, jegatheesan.r@ktr.srmuniv.ac.in

DOI: 10.15598/aeee.v15i5.2436

Abstract. *This paper proposes a new Switched Inductor based Quadratic Boost (SLQB) converter. The theoretical study for control design is carried out in detail. Small signal dynamic analysis of the proposed topology is obtained by State-Space averaging technique to investigate the closed-loop performance of SLQB converter. Ziegler-Nichols' closed loop tuning method is adapted to design the controller and analyze the closed loop performance. The theoretically derived transfer functions divulged a perfect matching with simulation results obtained from circuit simulator, spice. The effectiveness and adaptability of the SLQB converter are confirmed with high gain DC-DC converters belonging to the SL family. The stability study is carried out by MATLAB software, and the respective graphs are obtained to analyze the open loop and closed loop performance of the derived converter.*

Keywords

Poles, step response, Switched Inductor based Quadratic Boost (SLQB) converter, time domain analysis, transfer function, zeroes.

1. Introduction

Recently, DC-DC converters are operating as power optimizers in Renewable Energy System (RES). In that application, it is required to increase the boosting capability of the converter. Hence, the need of novel, efficient and reliable topology of the high gain DC-DC converter is increasing day by day. DC-DC converters are also used extensively in several applications such as computers, telecommunication, automobiles, medical instruments, military and various industrial applications. In most of these applications, DC distribution system is the most important part, and it is necessary to ensure the stability of the regime for the efficient operation. Stability analysis is not only used to design the controller but also allows the researchers to precisely understand the circuit operation. Several modeling techniques are reported in the literature for the DC-DC converter operating in continuous and discontinuous conduction mode. Most commonly used modeling techniques for DC-DC converters are PWM switch modeling [1], Current Injected Equivalent Circuit Approach (CIECA) [2] and [3], Modeling using Mason's gain formula [4], alternate PWM switch modeling [5] and [6], unified topological approach [7], signal flow graph modeling [8] and [9] and so on.

Many research works have been published in the area of stability analysis of DC-DC converter. However, certain issues are to be addressed [10]. Even though many methods are proposed for the dynamic analysis of DC-DC converter, it has been observed that State-Space Averaging (SSA) technique is the most suitable for small signal analysis. AC and DC transfer function of a converter can be easily obtained using SSA technique. In last decade, researchers have been concentrating on deriving several topologies for getting high gain and bi-directional flow of power. For many high gain topologies, stability analysis is not carried out owing to the increase in a number of passive components. In this work, we analyze a high gain DC-DC converter with State-Space averaging approach and results are validated by simulating the converter in circuit simulator like Pspice. Later, PI (Proportional and Integral) controller is designed for the proposed converter, and the KP and KI values are obtained by Ziegler-Nichols' tuning methods.

This paper is arranged as follows: The function of the proposed converter is discussed in Sec. 2. SLQB

converter is analyzed by steady-state analysis, and it is presented in Sec. 3. Section 4. describes the modeling of the converter by state space averaging approach. Section 5. gives the design of controller with time domain analysis. The advantage of the proposed converter and simulation results are provided in Sec. 6. Finally, the paper is concluded in Sec. 7.

1.1. Nomenclature

- SL : switched inductor,
- Vg : Input voltage,
- R_L : Load resistance,
- SW : Switch,
- V_{L1} : Voltage across inductor L_1,
- V_{L21} : Voltage across inductor L_{21},
- V_C : Voltage across capacitor C,
- I_{L1} : current through the inductor L_1,
- I_{L21} : current through the inductor L_{21},
- D - Duty cycle,
- f_s : Switching frequency,
- V_o : Output voltage,
- $\frac{\widetilde{v_o}(s)}{\widetilde{v_g}(s)}$: Input to output transfer function,
- $\frac{\widetilde{v_o}(s)}{\widetilde{d}(s)}$: Control to output transfer function,
- HID : High-Intensity Discharge lamp.

2. Proposed Topology

The derived topology can be used for powering HID lamps in automobile headlights. The steady state operating voltage of this lamp is around 80–100 V. A conventional boost converter cannot boost the voltage to the required level. Hence, the high gain

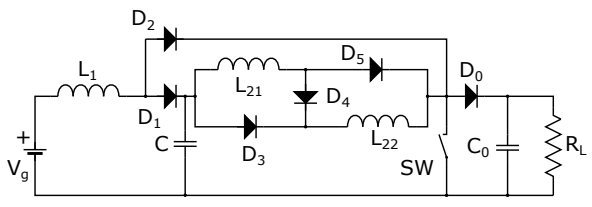

Fig. 1: SLQB converter.

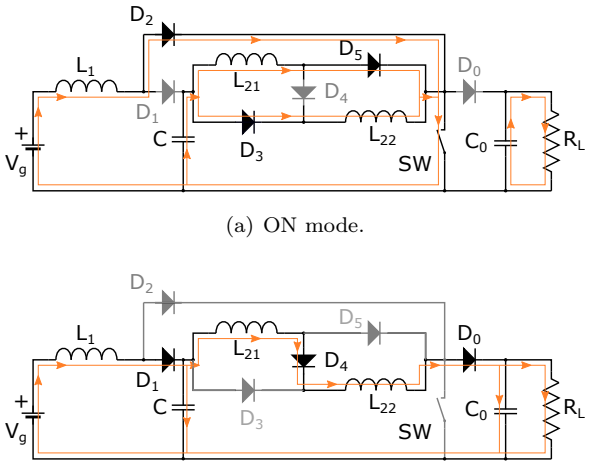

(a) ON mode.

(b) OFF mode.

Fig. 2: Modes of operation.

DC-DC converter is essential in this application. Figure 1 presents the topology obtained by incorporating the Switched Inductor cell with the quadratic boost converter. Switched inductor cell consists of two inductors (L_{21} and L_{22}) and three diodes (D_3, D_4, and D_5). The addition of SL cell in the QB converter increases the gain of the converter. Figure 2(a) and Fig. 2(b) show the ON and OFF mode of the proposed converter.

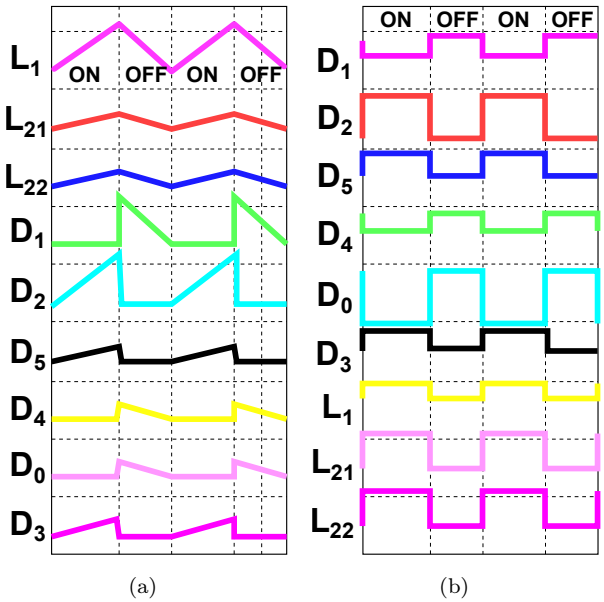

Fig. 3: (a) current through the components in the proposed converter, (b) voltage across the components in SLQB converter.

Mode(a): Figure 2(a) gives the current flow path of SLQB converter in ON mode. The operation of this mode is similar to the quadratic boost converter operation in ON mode. Inductor L_{21} and L_{22} are charged with the capacitor voltage V_c through the diode D_3,

D_5 and switch SW. In SL cell, diode D_4 is reversed biased by the voltage across the inductor in the SL cell. The output voltage is delivered to the load from the output capacitor C_O.

Mode(b): Figure 2(b) presents the current flow path of SLQB converter in OFF mode. In this discharging mode of the inductors, the diode D_3 and D_5 are blocked due to the polarity of the voltage across the inductor L_{21} and L_{22}. The output voltage is equal to the summation of the voltage across the inductors and capacitor. The addition of inductor in QB converter increases the gain to 1+D times of the gain of QB converter. Figure 3(a) and Fig. 3(b) present the waveform for the current through the elements and the voltage across the elements respectively.

3. Analysis of SLQB Converter

3.1. Steady State Analysis of SLQB Converter

The voltage conversion ratio of SLQB converter is obtained as follows Voltage across the inductor L_1 at ON and OFF condition is

$$V_{L1} = V_g, \tag{1}$$

$$V_{L1} = V_g - V_C. \tag{2}$$

Voltage across the inductor L_{21} and L_{22} at ON and OFF condition is

$$V_{L21} = V_{L22} = V_g, \tag{3}$$

$$V_{L21} = V_{L22} = \frac{V_C - V_O}{2}. \tag{4}$$

Combining the Eq. (1) with Eq. (2) and Eq. (3) with Eq. (4) by volt-sec principle, the following expressions are obtained.

$$V_C = \frac{V_g}{1-D}, \tag{5}$$

$$\frac{V_O}{V_g} = \frac{1+D}{[1-D]^2}. \tag{6}$$

Equation (6) gives the voltage gain of SLQB converter. Ampere-sec balance principle is applied to obtain the inductor current expression for the proposed converter. The expression for the current through the inductor is

$$I_{L1} = \frac{[1+D]\, I_O}{[1-D]^2}, \tag{7}$$

$$I_{L21} = I_{L22} = \frac{I_O}{1-D}. \tag{8}$$

3.2. Design of Inductor and Capacitator

Input inductor current at the CCM (Continuous Conduction Mode)/DCM (Discontinuous Conduction Mode) boundary is

$$I_{L1} = \frac{\Delta i_{L1}}{2} = \frac{i_{L1}(DT)}{2} = \frac{V_g DT}{2L_1}, \tag{9}$$

$$L_1 = \frac{R_L[1-D]^4 D}{2[1+D]^2 f_s}. \tag{10}$$

Switched inductor current at the CCM/DCM boundary is

$$I_{L21} = I_{L22} = \frac{\Delta i_{L21}}{2} = \frac{i_{L21}(DT)}{2} = \frac{V_g DT}{2[1-D]L_{21}}, \tag{11}$$

$$L_{21} = L_{22} = \frac{R_L[1-D]^2 D}{2[1+D]f_s}. \tag{12}$$

Equation (10) and Eq. (12) give the inductor design equations, and the value of inductor can be determined for various duty cycle and load resistance. The design equation for capacitors C and C_O is given in the Eq. (13) and Eq. (14).

$$C = \frac{V_O D}{R_L[1-D]f_s \Delta V_C}, \tag{13}$$

$$C_O = \frac{V_O D}{2R_L f_s \Delta V_{CO}}. \tag{14}$$

4. State-Space Averaging Technique

The general state space representation of a system is given by

$$\dot{x}(t) = Ax(t) + Bu(t), \tag{15}$$

$$y(t) = Cx(t) + Du(t). \tag{16}$$

Equation (15) and Eq. (16) describe the state and output equation respectively. The state space equation for SLQB converter for ON and OFF condition is

$$\dot{x}(t) = A_1 x(t) + B_1 u(t), \tag{18}$$

$$\begin{pmatrix} \dot{i_{L1}} \\ \dot{i_{L2}} \\ \dot{v_C} \\ \dot{v_{CO}} \end{pmatrix} = \begin{pmatrix} 0 & 0 & 0 & 0 \\ 0 & 0 & \frac{1}{L_{21}} & 0 \\ 0 & \frac{-2}{C} & 0 & 0 \\ 0 & 0 & 0 & \frac{-1}{R_L C_O} \end{pmatrix} \cdot \begin{pmatrix} i_{L1} \\ i_{L2} \\ v_C \\ v_{CO} \end{pmatrix} + \begin{pmatrix} \frac{1}{L_1} \\ 0 \\ 0 \\ 0 \end{pmatrix} (v_g), \tag{19}$$

$$\begin{pmatrix} \widetilde{i_{L1}} \\ \widetilde{i_{L2}} \\ \widetilde{v_C} \\ \widetilde{v_{CO}} \end{pmatrix} = \begin{pmatrix} 0 & 0 & \frac{-D'}{L_1} & 0 \\ 0 & 0 & \frac{1+D}{2L_{21}} & \frac{-D'}{2L_{21}} \\ \frac{D'}{C} & \frac{-[1+D]}{C} & 0 & 0 \\ 0 & \frac{D'}{C_O} & 0 & \frac{-1}{R_L C_O} \end{pmatrix} \begin{pmatrix} \widetilde{i_{L1}} \\ \widetilde{i_{L2}} \\ \widetilde{v_C} \\ \widetilde{v_{CO}} \end{pmatrix} + \begin{pmatrix} \frac{V_C}{L_1} & \frac{1}{L} \\ \frac{V_C+V_{CO}}{2L_{21}} & 0 \\ \frac{-(I_{L1}+I_{L21})}{C} & 0 \\ \frac{-I_{L21}}{C_O} & 0 \end{pmatrix} \begin{pmatrix} \widetilde{d} \\ \widetilde{v_g} \end{pmatrix}. \quad (17)$$

$$\dot{x}(t) = A_2 x(t) + B_2 u(t), \quad (20)$$

$$\begin{pmatrix} \dot{i}_{L1} \\ \dot{i}_{L2} \\ \dot{v}_C \\ \dot{v}_{CO} \end{pmatrix} = \begin{pmatrix} 0 & 0 & \frac{-1}{L_1} & 0 \\ 0 & 0 & \frac{1}{2L_{21}} & \frac{-1}{2L_{21}} \\ \frac{1}{C} & \frac{-1}{C} & 0 & 0 \\ 0 & \frac{1}{C_O} & 0 & \frac{-1}{R_L C_O} \end{pmatrix} \cdot \begin{pmatrix} i_{L1} \\ i_{L2} \\ v_C \\ v_{CO} \end{pmatrix} + \begin{pmatrix} \frac{1}{L_1} \\ 0 \\ 0 \\ 0 \end{pmatrix} (v_g), \quad (21)$$

$$y(t) = C_1 x(t) + D_1 u(t), \quad (22)$$

$$y(t) = C_2 x(t) + D_2 u(t), \quad (23)$$

$$(v_O) = \begin{pmatrix} 0 & 0 & 0 & 1 \end{pmatrix} \begin{pmatrix} i_{L1} \\ i_{L2} \\ v_C \\ v_{CO} \end{pmatrix} + (0)(v_g). \quad (24)$$

State system matrix (**A**), input matrix (**B**), output matrix(**C**) and feed forward matrix (**D**) of the converter is determined by considering the duty cycle, **D**.

$$\mathbf{A} = A_1 \mathbf{D} + A_2 (1 - \mathbf{D}), \quad (25)$$

$$\mathbf{B} = B_1 \mathbf{D} + B_2 (1 - \mathbf{D}), \quad (26)$$

$$\mathbf{A} = \begin{pmatrix} 0 & 0 & \frac{-\mathbf{D}'}{L_1} & 0 \\ 0 & 0 & \frac{1+\mathbf{D}}{2L_{21}} & \frac{-\mathbf{D}'}{2L_{21}} \\ \frac{\mathbf{D}'}{\mathbf{C}} & \frac{-[1+\mathbf{D}]}{\mathbf{C}} & 0 & 0 \\ 0 & \frac{\mathbf{D}'}{C_O} & 0 & \frac{-1}{R_L C_O} \end{pmatrix}, \quad (27)$$

$$\mathbf{B} = \begin{pmatrix} \frac{1}{L_1} \\ 0 \\ 0 \\ 0 \end{pmatrix}, \quad (28)$$

$$\mathbf{C} = \begin{pmatrix} 0 & 0 & 0 & 1 \end{pmatrix}, \quad (29)$$

$$\mathbf{D} = (0). \quad (30)$$

4.1. Steady State Model

For both steady state and small signal analysis, following assumptions are taken into consideration:

- Parasitic resistance of inductor and capacitor are neglected.
- Switch on state resistance is not considered.
- Forward voltage drop of the diodes is neglected.

The steady-state model of the converter is determined by considering only DC terms. All the time domain terms are replaced by the DC terms and the differentiating term is made zero.

$$0 = AX + BU. \quad (35)$$

Equation (35) is arranged to obtain X, and it is substituted in the output equation.

$$0 = -CA^{-1}BU. \quad (36)$$

All the matrices like **A**, **B** and **C** are substituted in Eq. (36) and solved to verify the voltage conversion ratio of SLQB converter.

$$V_O = \frac{-2L_1 L_{21} C C_O}{D'^4} \cdot \left[\frac{-(1+D)D'^2}{2L_{21} C C_O} \right] \cdot \frac{1}{L_1} \cdot V_g, \quad (37)$$

$$\frac{V_O}{V_g} = \frac{1+D}{[1-D]^2}. \quad (38)$$

By solving Eq. (37), it is verified that the Eq. (38) is same as that of Eq. (6) which is obtained from volt-sec balance principle.

4.2. Small Signal Model

By applying perturbations, the overall state and output equation of the converter is obtained Eq. (17).

The input to output voltage and duty cycle to output voltage transfer function is obtained as follows

$$\dot{x}(t) = Ax(t) + Bu(t). \quad (39)$$

$$\frac{\widetilde{v_O(s)}}{\widetilde{v_g}(s)} = \begin{pmatrix} 0 & 0 & 0 & 1 \end{pmatrix} \begin{pmatrix} s & 0 & \frac{D'}{L_1} & 0 \\ 0 & s & \frac{-(1+D)}{2L_{21}} & \frac{D'}{2L_{21}} \\ \frac{-D'}{C} & \frac{1+D}{C} & s & 0 \\ 0 & \frac{-D'}{C_O} & 0 & s+\frac{1}{R_L C_O} \end{pmatrix}^{-1} \begin{pmatrix} \frac{1}{L_1} \\ 0 \\ 0 \\ 0 \end{pmatrix}. \tag{31}$$

$$\frac{\widetilde{v_O(s)}}{\widetilde{v_g}(s)} = \frac{1+D}{[1-D]^2} \cdot \frac{1}{\left[\begin{array}{l} 1+s\left\{\frac{[1+D]^2 L_1}{[1-D]^4 R_L}+\frac{2L_{21}}{[1-D]^2 R_L}\right\}+s^2\left\{\frac{[1+D]^2 L_1 C_O}{[1-D]^4}+\frac{L_1 C}{[1-D]^2}+\frac{2L_{21}C_O}{[1-D]^2}\right\}+\ldots \\ \qquad \ldots+s^3\left\{\frac{2L_1 L_{21} C}{[1-D]^4 R_L}\right\}+s^4\left\{\frac{2L_1 L_{21} C C_O}{[1-D]^4}\right\} \end{array}\right]}. \tag{32}$$

$$\frac{\widetilde{v_O(s)}}{\widetilde{d(s)}} = \begin{pmatrix} 0 & 0 & 0 & 1 \end{pmatrix} \begin{pmatrix} s & 0 & \frac{D'}{L_1} & 0 \\ 0 & s & \frac{-(1+D)}{2L_{21}} & \frac{D'}{2L_{21}} \\ \frac{-D'}{C} & \frac{1+D}{C} & s & 0 \\ 0 & \frac{-D'}{C_O} & 0 & s+\frac{1}{R_L C_O} \end{pmatrix}^{-1} \begin{pmatrix} \frac{V_C}{L_1} \\ \frac{V_C+V_{CO}}{2L_{21}} \\ \frac{-[I_{L1}+I_{L21}]}{C} \\ \frac{-I_{L21}}{C_O} \end{pmatrix}. \tag{33}$$

$$\frac{\widetilde{v_O(s)}}{\widetilde{d(s)}} = \frac{R_L\left[\begin{array}{l} -2s^3 L_1 L_{21} C I_{L21}+s^2 D'\left(V_C+V_{CO}\right) L_1 C-s\{(1+D)^2 I_{L21} L_1+\ldots \\ \quad \ldots+2D'^2 I_{L21} L_{21}+D'\left(1+D\right) L_1\left[I_{L1}+I_{L21}\right]\}+D'^2\left[\left(1+D\right) V_C+D'\left(V_C+V_{CO}\right)\right] \end{array}\right]}{\begin{array}{r} 2L_1 L_{21} C R_L C_O s^4+2L_1 L_{21} C s^3+s^2\left\{(1+D)^2 L_1 R_L C_O+D'^2 L_1 C R_L+D'^2 2L_{21} R_L C_O\right\}\ldots \\ \ldots+s\left\{(1+D)^2 L_1+2D'^2 L_{21}\right\}+D'^4 R_L \end{array}}. \tag{34}$$

Take Laplace transform for the Eq. (39)

$$x\left(s\right) = [sI-A]^{-1} B u(s). \tag{40}$$

Substitute Eq. (40) in the output equation to determine the transfer function

$$y\left(s\right) = C[sI-A]^{-1} B u(s). \tag{41}$$

1) Input to Output Voltage Transfer Function

Substitute **A**, **B** and identity matrix in the equation Eq. (41) and determine input to output transfer function. $\widetilde{d(s)}$ is made zero to determine the $\frac{\widetilde{v_O(s)}}{\widetilde{v_g}(s)}$.

2) Duty Cycle to Output Voltage Transfer Function

Again to determine the control to output voltage transfer function $\widetilde{v_g}(s)$ is made zero Eq. (33).

Duty cycle to output transfer function Eq. (34).

Equation (32) and Eq. (34) give the input to output transfer function and control to output transfer function respectively, and it is used to design the voltage feedback compensation.

To determine the stability of the system, following parameters are used. V_g = 12 V, V_o = 96 V, R_L = 230 Ω, f_s = 60 kHz, D = 0.558. The reason for this operating voltage for the proposed converter is that the converter is designed for xenon lamp application. The power rating of the xenon lamp for this application is around 35–40 W.

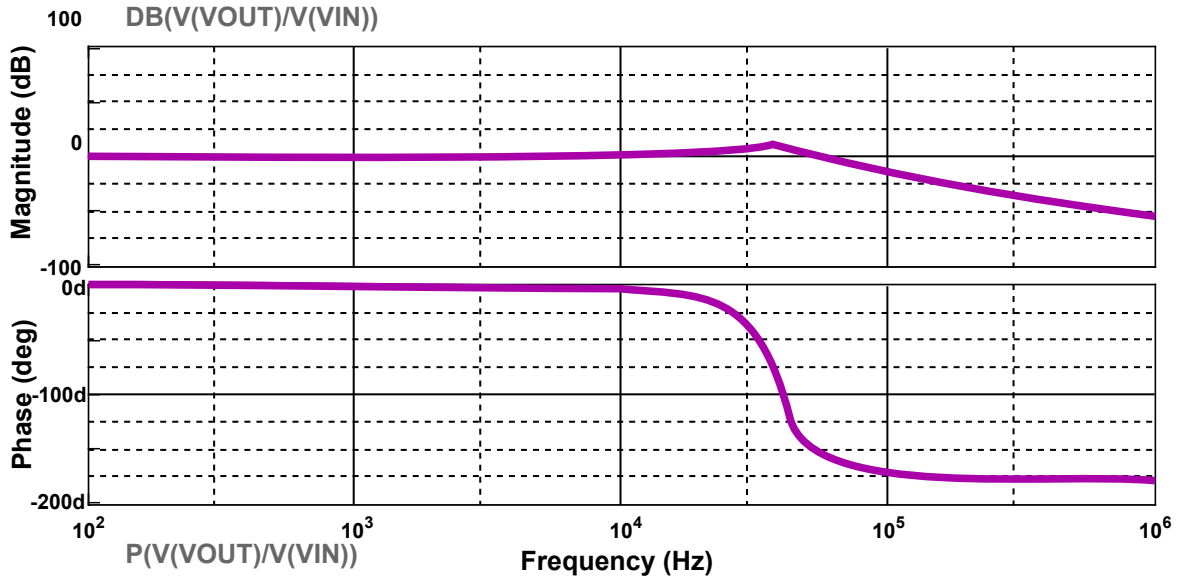

(a) Magnitude and phase plot obtained from Spice.

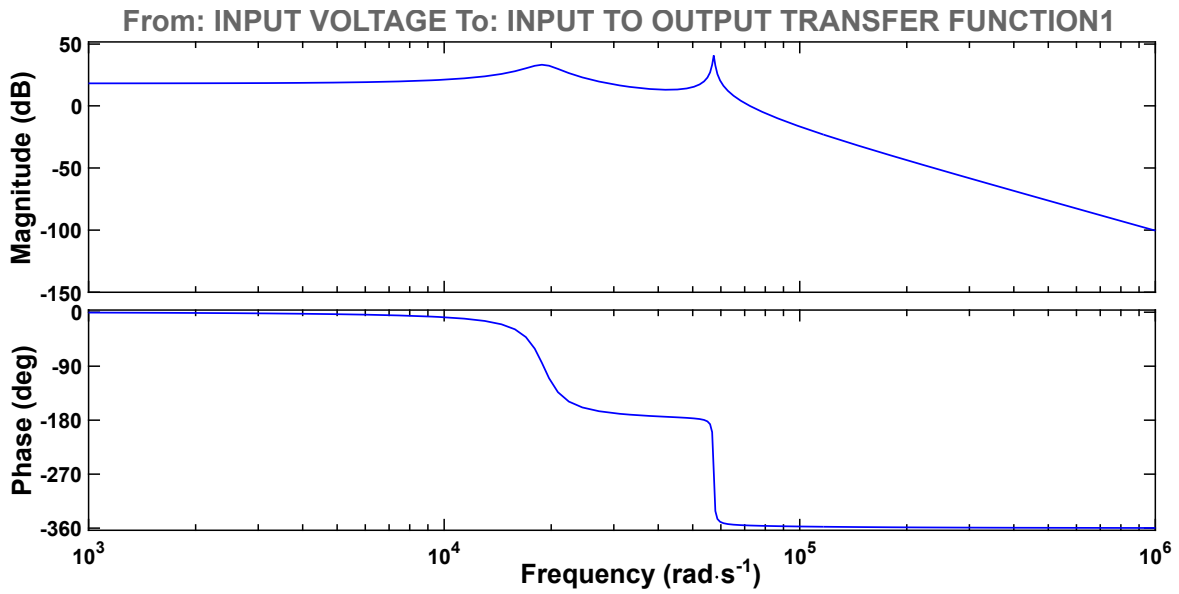

(b) Magnitude and phase plot obtained from derived transfer.

Fig. 4: Bode plot of Open-loop input to output transfer function.

Hence, the passive components of the converters are designed for 40 W, 96 V output voltage with 60 kHz switching frequency.

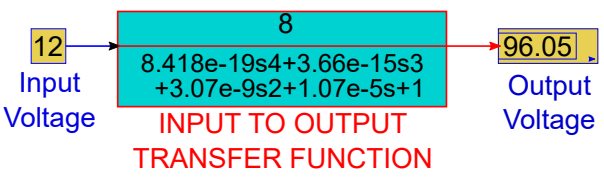

Fig. 7: Input to output transfer function in MATLAB/Simulink.

The values of passive components in the converter are L_1 =17 µH, L_{21} = L_{22} = 135 µH, C = 7 µF and C_O = 1 µF. Figure 4(a) presents the Bode plot of SLQB converter obtained from Pspice software, and it closely matches with the Bode plot drawn from the derived transfer function which is given in Fig. 4(b). Step response of open loop converter from MATLAB is provided in Fig. 5(a), and Fig. 5(b) shows the pole-zero map of the same. Stability and convergence rate of the system is affected by the location of the poles in the right and left half of the s-plane. Step response of open loop system tells us that the system has the very

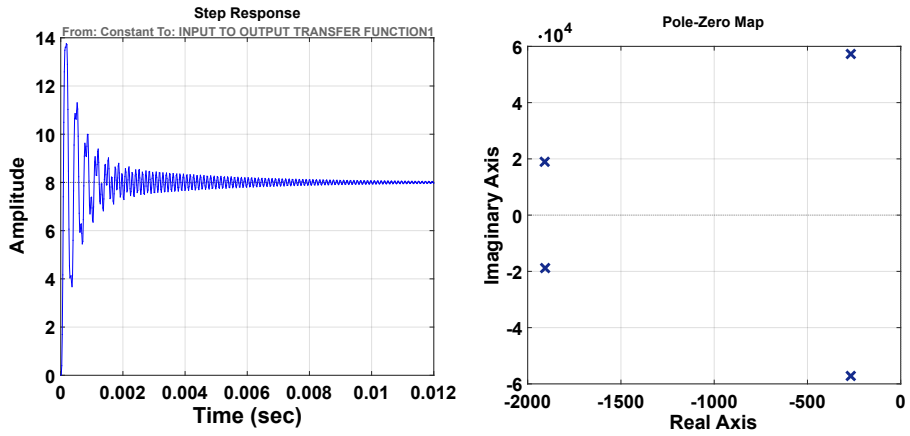

(a) (b)

Fig. 5: (a) Step response of open loop SLQB converter, (b) Pole-zero map of open loop SLQB converter.

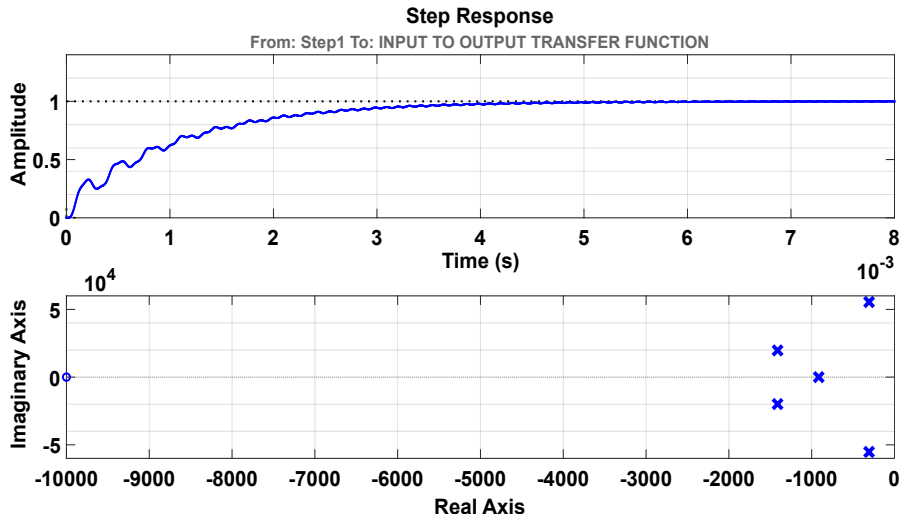

Fig. 6: Step response and pole-zero map of closed loop SLQB converter.

fast response but poor stability. The transfer function is simulated in MATLAB/Simulink to prove the output voltage, and it is given in Fig. 7.

Tab. 1: Ziegler-Nichols' closed loop tuning method.

Ziegler-Nichols' tuning		
PI Controller	K	T_i
	$0.4K_u$	$0.8T_u$

5. Design of Controller and Time Domain Analysis

Ziegler-Nichols' closed loop tuning method is used to tune PI controller. An open loop system is converted to the closed system, and gain is added to the system until there is a sustained oscillation in response to the step input. Let T_u be the ultimate period of the sustained oscillation and K_u is the ultimate gain which causes this sustained oscillation.

Table 1 gives the formula for the controller parameters in the Ziegler-Nichols' closed loop tuning method. Using this approach, PI parameters are determined, and GPI(s) is obtained.

$$G_{PI}(s) = \frac{0.125S + 125}{S}. \tag{42}$$

Equation (42) is cascaded with Eq. (32) to get a closed loop system and its step response and pole-zero map are obtained and given in Fig. 6.

A good perceptive of the time domain behavior of SLQB converters is accomplished. Table 2 gives the comparative study of time domain behavior of the converter between the open loop and closed condition. It

Tab. 2: Time domain analysis of SLQB converter.

Input to output transfer function	Poles	Zeros	Time domain specification
Open loop transfer function	$-3.27 \cdot 10^3 + \mathrm{i}2.3 \cdot 10^4$ $-3.27 \cdot 10^3 - \mathrm{i}2.3 \cdot 10^4$ $1.1 \cdot 10^3 + \mathrm{i}4.61 \cdot 10^4$ $1.1 \cdot 10^3 - \mathrm{i}4.61 \cdot 10^4$	NIL	Overshoot = 71 %, Rise time = 0.04 ms, Settling time = 6.6 ms.
Closed loop transfer function with PI controller	$-308 + \mathrm{i}5.69 \cdot 10^4$ $-308 - \mathrm{i}5.69 \cdot 10^4$ $-1.41 \cdot 10^3 + \mathrm{i}2 \cdot 10^4$ $-1.41 \cdot 10^3 - \mathrm{i}2 \cdot 10^4$ -915	$-1 \cdot 10^4$	Overshoot = 0 %, Rise time = 2.3 ms, Settling time = 4.3 ms.

Tab. 3: Comparison of SLQB converter with hybrid POEL converter [11].

Parameter	SLQB converter	Hybrid POEL converter with the basic SI cell [11]	Hybrid POEL converter with the self-lift SI cell [11]	Hybrid POEL converter with the double self-lift SI cell [11]
Voltage gain	$\frac{1+D}{[1-D]^2}$	$\frac{D+D}{1-D}$	$\frac{2D}{1-D}$	$\frac{3D-D^2}{1-D}$
Switch voltage stress	$\frac{[1+D]V_g}{[1-D]^2}$	$\frac{[1+D]V_g}{1-D}$	$\frac{2V_g}{1-D}$	$\frac{[3-D]V_g}{1-D}$
No of switch	1	1	1	2
No of diode	6	4	5	5
No of inductor	3	3	3	3
No of capacitor	2	2	3	4

is observed from the simulation results that the overshoot has reduced to 0 % with the PI controller. The result also shows that there is a substantial decrease in the settling time with the closed loop system. The rise time is not reduced in closed loop compared to open loop system.

6. Advantage of the Proposed Converter and Simulation Results

In this section, comparison is carried out with the existing converter in the literature to emphasize the advantage of the SLQB converter. The superiority of SLQB converter is proved by comparing the converter with hybrid POEL converter [11], and it is tabulated in Tab. 3. The converter's advantage is analyzed with the same parameters used for stability analysis.

From the analysis, it is observed that to achieve 96 V output voltage from 12 V DC supply, hybrid POEL converter with primary SI cell, self-lift cell and double self-lift cell [11] requires a duty cycle of 0.815, 0.8 and 0.783 respectively. However, SLQB converter gives the same output voltage with $D = 0.558$. The proposed topology requires on an average only 70 % of the duty cycle needed for the hybrid POEL converter. With switch voltage stress analysis, it has been found

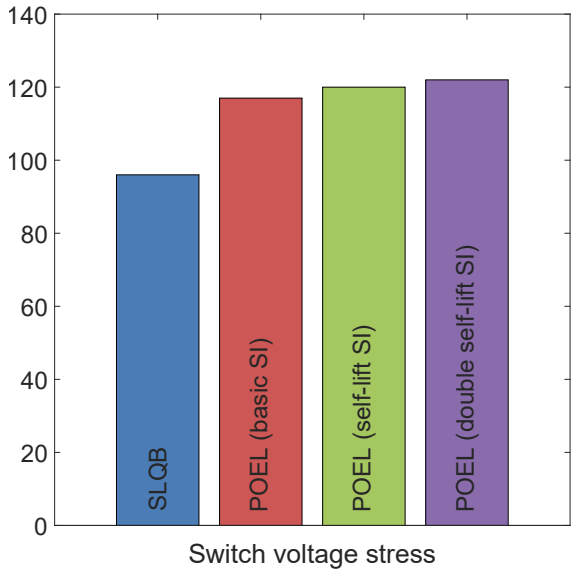

Fig. 9: Comparison of Switch voltage stress.

that the hybrid POEL converter with basic SI cell, self-lift cell, and double self-lift cell [11] suffers from a voltage stress of 117 V, 120 V, and 122 V respectively for the same input and output data. The proposed topology has a single switch with the voltage stress equal to the output voltage (96 V). Number of components in the SLQB converter is 12 which is less in comparison

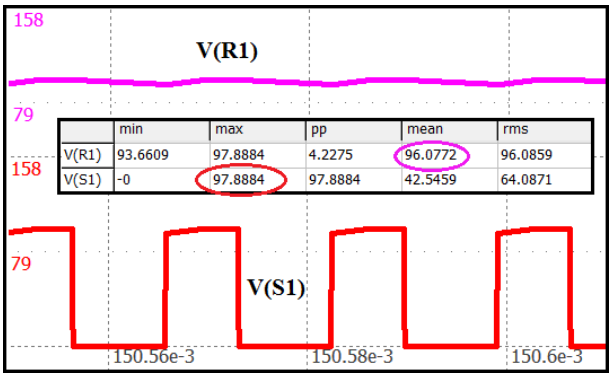

	min	max	pp	mean	rms
V(R1)	93.6609	97.8884	4.2275	96.0772	96.0859
V(S1)	-0	97.8884	97.8884	42.5459	64.0871

(a) Output voltage and switch stress voltage.

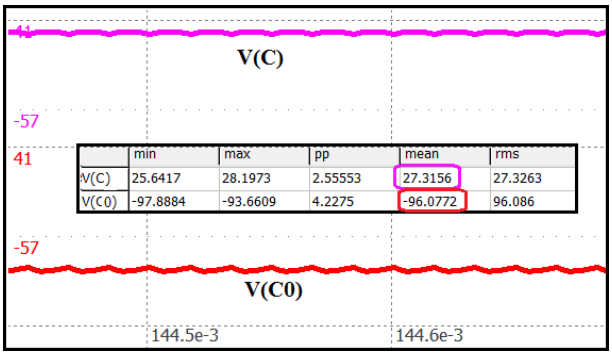

	min	max	pp	mean	rms
V(C)	25.6417	28.1973	2.55553	27.3156	27.3263
V(C0)	-97.8884	-93.6609	4.2275	-96.0772	96.086

(b) Switch current and output current.

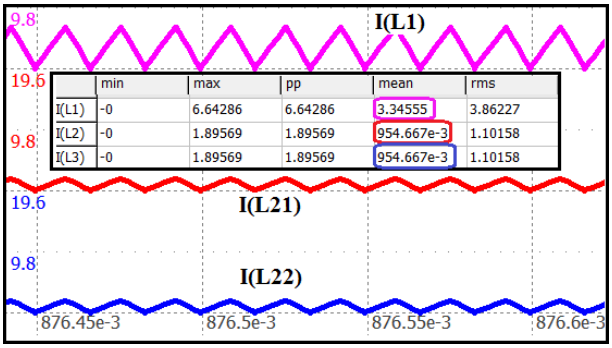

	min	max	pp	mean	rms
I(L1)	-0	6.64286	6.64286	3.34555	3.86227
I(L2)	-0	1.89569	1.89569	954.667e-3	1.10158
I(L3)	-0	1.89569	1.89569	954.667e-3	1.10158

(c) Voltage across the capacitor.

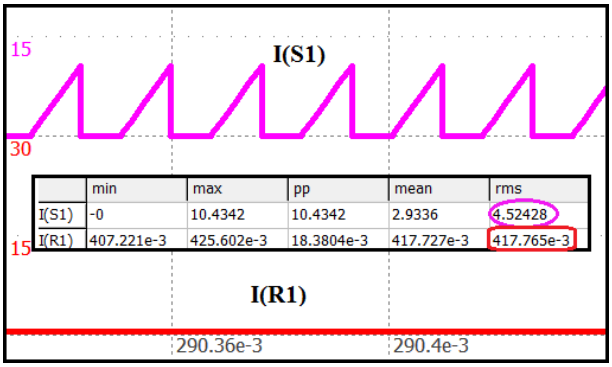

	min	max	pp	mean	rms
I(S1)	-0	10.4342	10.4342	2.9336	4.52428
I(R1)	407.221e-3	425.602e-3	18.3804e-3	417.727e-3	417.765e-3

(d) Inductor currents.

Fig. 8: Simulation results.

to hybrid POEL converter with double self-lift cell and same as that of the converter with the self-lift cell.

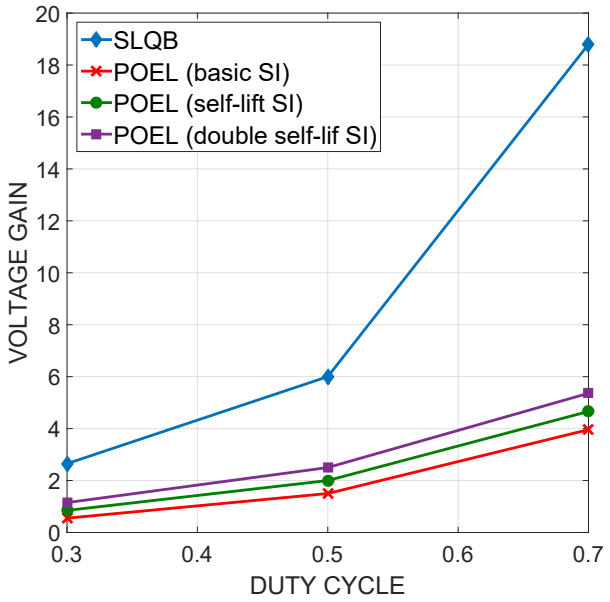

Fig. 10: Dutycycle vs Voltage gain.

The voltage gain of the proposed topology is compared with the converter in [11] for different duty cycle and its graphical comparison is shown in the Fig. 10. The voltage stress across the switch is calculated and compared. From Fig. 9, it is observed that the SLQB converter has less voltage stress for the chosen output voltage.

Figure 8 gives the simulation results obtained from the nL5 simulator. Figure 8(a) presents the output voltage and switch stress voltage. The results achieved from the nL5 matches with the theoretical results and it is tabulated in Tab. 4 with the formula. Switch current and output current is given in Fig. 8(b). Figure 8(c) and Fig. 8(d) show the waveform of capacitor voltages and inductor currents respectively. Figure 11 supplies the step response of both the system using MATLAB/Simulink. The response shows the improvement in time response with PI controller designed with Ziegler Nicholas' closed loop tuning method.

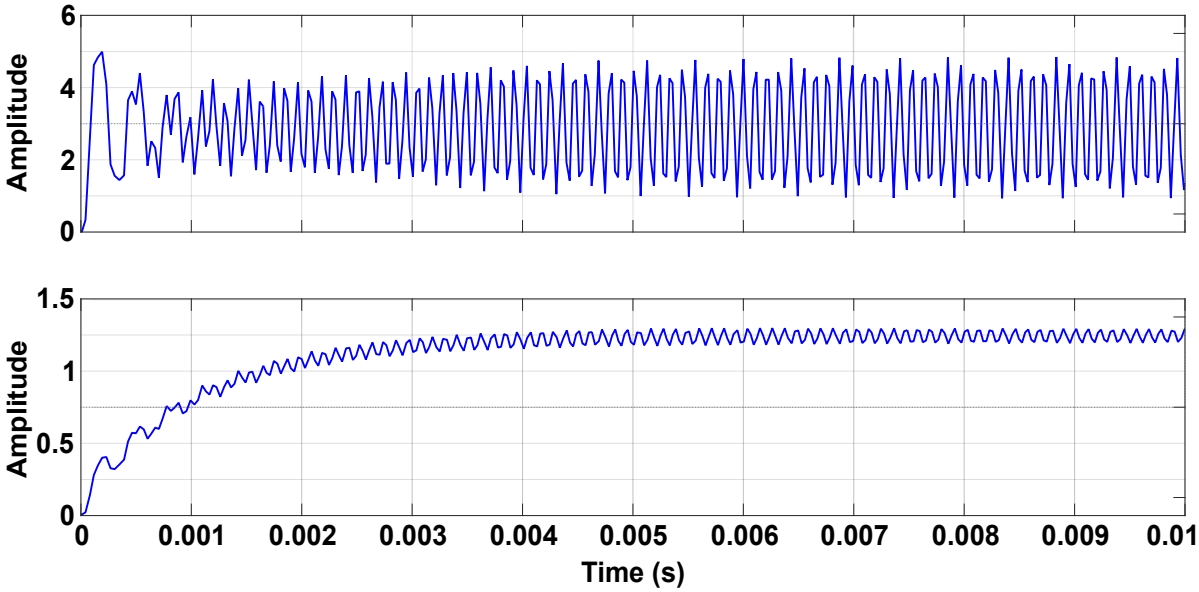

Fig. 11: Time domain response of SLQB Converter in open loop and closed loop condition.

Tab. 4: Theoretical analysis of SLQB converter.

SLQB converter: $V_g = 12$ V, $V_o = 96$ V, $R_L = 230\ \Omega$, $f_s = 60$ kHz, $D = 0.558$			
Parameter	**Theoretical formula**	**Theoretical result**	**Simulation result**
Output,voltage	$\frac{[1+D]V_g}{[1-D]^2}$	96 V	96 V
Switch voltage stress	V_o	96 V	97 V
QB capacitor voltage	$\frac{V_g}{1-D}$	27.2 V	27.3 V
Output capacitor voltage	V_o	96 V	96 V
Inductor current (L_1)	$\frac{[1+D]I_O}{[1-D]^2}$	3.33 A	3.34 A
Inductor current (L_{21})	$\frac{I_o}{1-D}$	0.95 A	0.954 A
Inductor current (L_{22})			
RMS switch current	$\frac{3I_o\sqrt{D}}{[1-D]^2}$	4.78 A	4.52 A
Output current	$\frac{V_o}{R_L}$	0.417 A	0.417 A

7. Conclusion

A complete frame of small-signal analysis for the open-loop SLQB converter and the controller design is carried out. Ziegler Nicholas' closed loop tuning is adapted for adjustment of P and I parameter and it is very convenient method compared to other tuning methods. The advantages of the proposed topology are

- High gain compared to the converter taken for the comparison.
- Low voltage stress across the semiconductor devices.

Stability of the converter is analyzed by State-Space averaging technique. Time response of the closed loop system shows good results with PI controller. Simulation is performed in nL5 simulator and Matlab software. The circuit is simulated in the nL5 and it matches with the results obtained from the steady-state analysis. Time domain response is obtained in Matlab software, and it matches with the results obtained from the State-Space averaging technique. The derived transfer function is verified with the Bode plot obtained from the circuit simulator, Spice. A high gain DC-DC converter is derived, and its steady-state and dynamic analysis is carried out. Finally, the theoretical results are validated with the results from simulation software.

References

[1] DIJK, E. V., H. J. N. SPRUIJT, D. M. O'SULLIVAN and J. B. KLAASSENS. PWM-Switch modeling of DC-DC Converters. *IEEE Transactions on Power electronics.* 1995, vol. 10, no. 6, pp. 659–665. ISSN 0885-8993. DOI: 10.1109/63.471285.

[2] CHETTY, P. R. K. Current Injected Equivalent Circuit Approach to Modeling Switching DC-DC Converters. *IEEE Transactions on Aerospace and Electronic Systems.* 1981, vol. AES-17, no. 6, pp. 802–808. ISSN 0018-9251. DOI: 10.1109/TAES.1981.309131.

[3] CHETTY, P. R. K. Current Injected Equivalent Circuit Approach to Modeling Switching DC-DC Converters in discontinuous inductor conduction mode. *IEEE Transactions on industrial electronics.* 1982, vol. IE-29, no. 3, pp 230–234. ISSN 0278-0046. DOI: 10.1109/TIE.1982.356670.

[4] WONG, L. K. and T. K. MAN. Small signal modeling of open-loop SEPIC converters. *IET Power Electronics.* 2010. vol. 3, no. 6, pp. 858–868. ISSN 1755-4535. DOI: 10.1049/iet-pel.2009.0300.

[5] NGO, K. D. T. Alternate form of the PWM switch model. *IEEE Transactions on Aerospace and Electronic system.* 1999, vol. 3, no. 6, pp 1283–1292. ISSN 1755-4535. DOI: 10.1109/7.805445.

[6] CHEN, J. and K. D. T. NGO. Alternate forms of the PWM switch model in discontinuous conduction mode. *IEEE Transactions on Aerospace and Electronic Systems.* 2001, vol. 37, no. 2, pp. 754–758. ISSN 0018-9251. DOI: 10.1109/7.937489.

[7] PIETKIEWICZ, A. and D. TOLLIK. Unified Topological Modeling Method Of Switching DC-DC Converters In Duty-Ratio Programmed Mode. *IEEE Transactions On Power Electronics.* 1987, vol. Pe-2, no. 3, pp. 218–226. ISSN 0885-8993. DOI: 10.1109/TPEL.1987.4766362.

[8] VEERACHARY, M. General rules for signal flow graph modeling and analysis of dc-dc converters. *IEEE Transactions on Aerospace and Electronic Systems.* 2004, vol. 40, no. 1, pp. 259–271. ISSN 0018-9281. DOI: 10.1109/TAES.2004.1292158.

[9] VEERACHARY, M. Signal flow graph modelling of multi-state boost DC-DC converters. *IEE Proceedings - Electric Power Applications.* 2004, vol. 151, no. 5, pp. 583–589. ISSN 1350-2352. DOI: 10.1049/ip-epa:20040680.

[10] AROUDI, A. E., D. GIAOURIS, H. H.-C. IU and I. A. HISKENS. A Review on Stability Analysis Methods for Switching Mode Power Converters. *IEEE Journal on Emerging and Selected Topics in Circuits and Systems.* 2015, vol. 5, no. 3, pp 302–315. ISSN 2156-3357. DOI: 10.1109/JETCAS.2015.2462013.

[11] JIAO, Y., F. L. LUO and M. ZHU. Voltage-lift-type switched-inductor cells for enhancing DC-DC boost ability: principles and integrations in Luo converter. *IET Power Electron.* 2011, vol. 4, iss. 1, pp. 131–142. ISSN 1755-4535. DOI: 10.1049/iet-pel.2010.0021.

[12] FFmpeg tool. In: *FFmpeg* [online]. 2017. Available at: `https://www.ffmpeg.org/`.

About Authors

Divya Navamani JAYACHANDRAN she received the B.E. degree from Madras University and the M.E. degree from Sathyabama University in power electronics and Industrial drives. She is currently working in the area of high gain DC-DC converter. Her research interests include power electronics, electric and hybrid electric vehicle DC-DC converter. She is the life member of IEI, ISTE.

Vijayakumar KRISHNASAMY He received the B.E. and M.E. degree from Annamalai University in Power systems. His research interests include Power system: Deregulation, Modeling, Control and Operation, Optimization, FACTS, Power Quality. He is a life member of IEI, ISTE.

Jegatheesan RAMIAH received the B.E. degree from Madras University and M.Sc. (Engg) in Power systems from Madras University. He completed his Ph.D. in the year 1975 from IIT, Kanpur. His research interests include large scale, Power system, power system optimization and state Estimation. He is a life member of ISTE.